

Pharmaceutical Nanotechnology

Superparamagnetic iron oxide nanoparticles stabilized by alginate: Pharmacokinetics, tissue distribution, and applications in detecting liver cancers

Hui Li Ma^a, Yu Feng Xu^b, Xian Rong Qi^{a,*}, Yoshie Maitani^c, Tsuneji Nagai^d

^a Department of Pharmaceutics, School of Pharmaceutical Sciences, Peking University, Beijing 100083, China

^b Department of Radiology, First Hospital, Peking University, Beijing 100034, China

^c Institute of Medicinal Chemistry, Hoshi University, Shinagawa-Ku, Tokyo 142-8501, Japan

^d The Nagai Foundation Tokyo, Hon-Komagome, Bunkyo-ku, Tokyo 113-0021, Japan

Received 13 August 2007; received in revised form 18 November 2007; accepted 20 November 2007

Available online 28 November 2007

Abstract

The objectives of this study were to describe the pharmacokinetics and tissue distribution of superparamagnetic iron oxide nanoparticle (SPIO) stabilized with alginate (SPIO-alginate), and investigate its potential in detecting liver cancers as a newly developed magnetic resonance (MR) contrast agent. Pharmacokinetics and tissue distribution of SPIO-alginate were investigated in Sprague–Dawley rats. The results showed that SPIO-alginate was eliminated rapidly from serum with the half-life of 0.27 h at 109.5 $\mu\text{mol Fe/kg}$ and accumulated dominantly in liver and spleen with a total percentage of more than 90% of dose after intravenous injection. The studies of pharmacokinetics and distribution of SPIO-alginate in rats indicated the MR contrast agent, based on SPIO, mainly accumulating in targeting organs that contain phagocytosing cells, i.e. liver and spleen. The efficacies in detecting hepatocellular carcinoma (HCC) of rat with primary liver cancer and xenograft liver cancers of rabbit were investigated before and after injection of SPIO-alginate. The signal intensity of liver parenchyma in rabbit with VX2 tumor after injection of SPIO-alginate was reduced sharply resulting in a significant contrast between liver parenchyma and tumor. Detection of the HCC in rat model was also demonstrated. The present study provides evidence that SPIO-alginate might have the ability to improve the detection of liver tumors as an MR contrast agent, and the efficacy is associated with the SPIO specifically located in Kupffer cells in hepatic sinusoid.

© 2007 Elsevier B.V. All rights reserved.

Keywords: Superparamagnetic iron oxide nanoparticles (SPIO); Pharmacokinetics; Distribution; Liver cancers; Contrast agent; Alginate

1. Introduction

MR imaging is one of the most useful non-invasive methods in the field of diagnostic imaging, which is characterized by its high resolution of soft-tissues and by its non-exposure to radiation. To better differentiate healthy and pathological tissues, paramagnetic gadolinium based contrast agents which shorten the longitudinal relaxation time (T1) and increase the contrast of the image (positive enhancement) are mainly used today (Weinmann et al., 2003). Compared to gadolinium based contrast agents, SPIO can produce enhanced relaxation rates in specific organs at lower dose than paramagnetic ions, because

of their larger magnetic moment (Corot et al., 2006; Wang et al., 2001). Generally speaking, the transverse relaxation (T2 and T2*) effect of SPIO is mostly utilized in detection of liver lesions by MR imaging. SPIO are distributed in reticuloendothelial cells, such as Kupffer cells (KCs), according to phagocytic activity, and cause local field inhomogeneities that produce rapid dephasing of neighboring proton spins, resulting in a shortening of T2 relaxation times. In contrast, liver tumors such as metastatic liver cancer and HCC cannot absorb these agents because of the lack of reticuloendothelial cells. Therefore, the contrast between tumor tissue and surrounding normal liver tissue is enhanced because of signal loss in the liver tissue (Saini et al., 1987). Hence, SPIO can produce a strong decrease in MR signal intensity (negative enhancement) in the tissues where they accumulate, such as the liver, spleen, bone marrow, and lymph node (Saini et al., 1987; Corot et al., 2006).

* Corresponding author. Tel.: +86 10 82801584; fax: +86 10 82802791.
E-mail address: qixr2001@yahoo.com.cn (X.R. Qi).

Until now, two SPIO preparations have already been approved for clinical use, especially for liver MR imaging, such as Ferumoxides (i.e. Endorem® in Europe, Feridex® in the USA and Japan, Advanced Magnetics, USA) coated with dextran (Weissleder et al., 1989), and Ferucarbutran (i.e. Resovist® in Europe and Japan, Schering, Germany) coated with carboxydextran (Reimer et al., 1995). Furthermore, several SPIO preparations have been investigated in human for imaging applications, such as VSOP-C184, a very small SPIO coated with citrate (Taupitz et al., 2004), and Feruglose (Clariscan; Amersham Health, Oslo, Norway) where iron oxide particles have been stabilized with oxidized starch that consist of carbohydrate-polyethylene glycol (Kellar et al., 2000).

In our previous work, SPIO stabilized with alginate (SPIO-alginate) have been successfully prepared (Ma et al., 2007) and the SPIO-alginate have good biocompatibility and some magnetic targeting under the magnetic field (Ma et al., 2007a). As the coating material of iron oxide, alginate is known for binding many multivalent ions *in vitro* such as Ca^{2+} , Ba^{2+} , Fe^{2+} , and Fe^{3+} . The high stability of SPIO-alginate is probably caused by the binding of the carboxyl group of alginate to iron oxide nuclei (Ma et al., 2007). It was reported that the absorption of Fe, Cr, and Co was significantly reduced after oral administration of sodium alginate in rats, while Ca and Zn absorption was not affected (Harmut-Hoene and Schelenz, 1980). Hence, it is necessary to investigate the effect of alginate and SPIO-alginate on the iron level *in vivo*, even if some COO^- terminals of alginate have been bound to iron oxide in SPIO-alginate.

We presumed that using SPIO-alginate as an intravenous contrast medium, detection of malignant liver lesions by MR imaging might be improved. Once iron oxide particles are taken up by the macrophages situated in the liver of reticuloendothelial system (RES) but not by tumor cells, the contrast between liver parenchyma and liver lesion would significantly increase, which is caused by the distinct signal loss in liver parenchyma and the almost stable signal intensity in malignant liver tumors (Saini et al., 1987; Clement et al., 1991; Nakayama et al., 1998; Imai et al., 2000; Bourrinet et al., 2006).

To investigate whether this highly stabilized SPIO-alginate is a kind of ideal MR contrast for liver imaging, the pharmacokinetics and tissue distribution of SPIO-alginate in rats were first examined in this study. After that, the efficacy of SPIO-alginate for the detection of liver cancers was evaluated in two kinds of tumor models, VX2 liver tumor in rabbit and primary liver cancer in rat.

2. Materials and methods

2.1. Contrast agent

Typical iron oxide nanoparticles were Fe_3O_4 with a core diameter of 5–10 nm. Meanwhile, SPIO-alginate had a hydrodynamic diameter of 193.8 nm with good stability as well as superparamagnetism, and its ξ -potential was -65.0 mV. T1 and T2 relaxivities of SPIO-alginate in physiological saline (1.5 T, 20 °C) were 7.86 ± 0.20 and $281.2 \pm 26.4 \text{ s}^{-1} \text{ mM}^{-1}$, respectively. Other properties of SPIO-alginate were described in detail

in the previous publication (Ma et al., 2007, 2007a). For MR imaging experiment, SPIO-alginate was diluted to a concentration of $8.9 \mu\text{mol Fe/mL}$ with physiological saline.

2.2. Pharmacokinetics, tissue distribution and histological evaluation in normal rats

Male Sprague–Dawley rats weighing 150 ± 20 g were purchased from Experimental Animal Center of Peking University, China. All care and handling of animals were performed with the approval of Institutional Authority for Laboratory Animal Care of Peking University, which followed the guidelines established by the China Council for Animal Care. The animals were anesthetized by intraperitoneal injection of 1.0 g/kg of ethyl carbamate. The pharmacokinetics studies (using whole blood) were carried out with 29 rats which were divided into four groups randomly. The rats were intravenously injected with the following formulations individually: SPIO-alginate at a dose of $109.5 \mu\text{mol Fe/kg}$ (SPIO-low dose) ($n=18$), SPIO-alginate at a dose of $218.9 \mu\text{mol Fe/kg}$ (SPIO-high dose) ($n=3$), 1 mL 0.6% (w/v) alginate solution (alginate solution) ($n=3$), and 1 mL physiological saline (saline) ($n=5$). About 0.3 mL blood samples were taken by retro-orbital venous plexus puncture at 0 min (before intravenous injection), 5 min, 10 min, 30 min, 1 h, 3 h, 6 h, 12 h, 24 h, 48 h, 96 h, 168 h, and 336 h after injection, respectively.

The pharmacokinetics studies (using serum) were obtained in rats by quantitative determination of iron in serum. Twenty rats were divided into four groups ($n=5$ per group) in random and injected with SPIO-low dose, SPIO-high dose, alginate solution, and saline, respectively. About 0.6 mL blood samples were collected from retro-orbital venous plexus puncture at 0 min, 5 min, 10 min, 30 min, 1 h, 3 h, 6 h, 12 h, and 24 h after injection, respectively. Then each clotted blood sample was centrifuged at 7000 rpm for 20 min to get serum sample.

The basic serum iron concentration was calculated from the average serum iron concentration at 0 min of all the rats. The serum iron concentrations at various time points after administration were calculated by subtracting the basic serum iron concentration. Serum iron concentration–time profiles were analyzed by WinNonlin computer software, Version 3.1 (Pharsight Corporation, Mountain View, CA), using noncompartmental method with bolus intravenously administration. The following parameters were obtained: maximum tissue concentration (C_{max}), elimination rate constant (λ), elimination half-life ($T_{1/2}$), area under the curve (AUC), and mean residence time (MRT).

The tissue distribution of SPIO-alginate at a dose of $109.5 \mu\text{mol Fe/kg}$ in rats (total 21) were studied at 0, 0.5, 3, 24, 48, 96, and 336 h after injection, which was performed simultaneously with the blood pharmacokinetics study of SPIO-low dose. Tissues of interest (blood, liver, spleen, heart, lungs, and kidneys) were collected immediately at various time points, weighted, and frozen at -20 °C until analysis.

Liver and spleen concentration–time profiles were analyzed by WinNonlin computer software using a noncompartmental method with a single extravascular dosing. The iron concentrations in liver and spleen at various time points were calculated

by subtracting the iron concentration in liver or in spleen at 0 h (before injection), respectively. The following parameters were obtained: time of maximum concentration (T_{\max}), C_{\max} , λ , $T_{1/2}$, AUC, and MRT.

Liver and spleen were removed at 0.5, 24, 96, and 336 h after injection of SPIO-low dose, and at 336 h after injection of SPIO-high dose and alginate solution, respectively. Then the samples were fixed in 4% paraformaldehyde solution (pH 7.4) for hematoxylin-eosin (HE) staining and Perls staining. The liver and spleen section specimens were examined under a light microscopy after staining.

2.3. Iron content measurement

For quantitative determination of iron content, blood, serum and tissue samples were digested in a beaker with the mixed acid of HNO_3 – HClO_4 (4:1, v:v) for 48 h at room temperature, and then evaporated to dryness at 100 °C by sand bath with electric hot plate. Finally 37.5% HCl solution was added to the beaker to dissolve the solid and the iron content was determined by *o*-phenanthroline method (Hagar et al., 2003).

2.4. Tumor models of rats and rabbits

Male Sprague–Dawley rats (130–140 g, total 35) were used. The model of primary liver cancer in rats ($n = 29$) was established by giving 70 mg diethylnitrosoamine (DENA, Sigma–Aldrich, USA) per kg weight 14 times at 7-d intervals through intra-gastric administration with physiological saline. As DENA was sensitive to light, a fresh solution was prepared for each administration and kept in dark bottles for short periods. The rats of control group ($n = 6$) were raised in the normal condition.

VX2 rabbit tumor was cut into small pieces (about 1 mm³), and then implanted into left hepatic lobe to establish single liver cancer in rabbit. After implantation, VX2 tumor rapidly developed in the liver and the implanted tumor formation was detected by computed tomography (CT) on week 2. The surgery and implantation procedures have been described in detail in the previous publication (Hauff et al., 1997).

2.5. MR imaging in normal rat

All MR imaging examinations were performed by using a clinical 3.0 T MR scanner (Signa Horizon, General Electric Medical Systems, Milwaukee, WI) with a surface coil. For the investigations of liver enhancement in normal rats, the normal rats ($n = 6$) were imaged before and after injection of SPIO-alginate at a dose of 20 $\mu\text{mol Fe/kg}$ through femoral vein. T1-weighted fast spin echo (FSE) or spoiled gradient-recalled (SPGR) sequence, T2-weighted fast recovery fast spin echo (FRFSE) sequence, and T2*-weighted gradient-recalled echo (GRE) sequence were used for the MR imaging. All the sequences were applied with a bandwidth of 31.25 kHz and slice thickness of 3 mm. Other parameters were as follows: T1-weighted FSE sequence (TE 14.6 ms; TR 800 ms; Echo train length 3; Matrix 288 \times 192; NEX 4; FOV 8 \times 8); T1-weighted SPGR sequence (TE 3.7 ms; TR 100 ms; Flip angles 60°;

Matrix 128 \times 128; NEX 6; FOV 8 \times 4); T2-weighted FRFSE sequence (TE 150 ms; TR 3000 ms; Echo train length 21; Matrix 128 \times 128; NEX 6; FOV 8 \times 5.6); T2*-weighted GRE sequence (TE 4.7 ms; TR 300 ms; Flip angles 15°; Matrix 128 \times 128; NEX 6; FOV 8 \times 4).

2.6. MR imaging in tumor animals and histological evaluation

For rabbits with VX2 tumor, unenhanced and enhanced T2*-weighted images were investigated before and after injection of SPIO-alginate at a dose of 20 $\mu\text{mol Fe/kg}$ using SPGR sequence with the following parameters: TR of 220 ms, TE of 5.2 ms, flip angles of 70°, slice thickness of 4 mm, slice gap of 1.0 mm, matrix of 512 \times 160, field of view of 13 \times 13, and bandwidth of 62.5 kHz.

For rats with primary liver cancer, unenhanced and enhanced images were obtained before and after injection of SPIO-alginate at a dose of 20 $\mu\text{mol Fe/kg}$ using T2*-weighted GRE sequence with the parameters just mentioned above in MR imaging for normal rats. The rats were sacrificed within 2–12 h after MR imaging evaluation. Then, liver specimens were fixed, the size, number, and shape of the lesions were observed, and the lesions were histologically identified after HE staining and Perls staining. The pathological changes e.g. hyperplastic nodules, cirrhotic and HCC, were also observed.

2.7. Imaging analysis

Quantitative analysis was performed by using an operator defined region of interest (ROI) of 6 mm² on T1-weighted, T2-weighted and T2*-weighted images, respectively. Major vessels were avoided when the signal intensities of liver parenchyma and tumor were measured. Measurements included signal intensity (SI) of the HCC (SI_{HCC}), the liver parenchyma without cirrhosis (SI_{liver}), the liver parenchyma with cirrhosis ($\text{SI}_{\text{cirrhosis}}$), and standard deviation of noise ($\text{S.D.}_{\text{noise}}$), respectively. Signal-to-noise ratio (SNR) was then calculated on both pre- and post-SPIO-alginate images by taking the SI_{HCC} , SI_{liver} or $\text{SI}_{\text{cirrhosis}}$ dividing by each $\text{S.D.}_{\text{noise}}$. In addition, contrast-to-noise ratio (CNR) was calculated with the following formula: $(\text{SI}_{\text{HCC}} - \text{SI}_{\text{cirrhosis}})/\text{S.D.}_{\text{noise}}$, and the relative contrast was expressed as $\text{SI}_{\text{HCC}}/\text{SI}_{\text{cirrhosis}}$.

3. Results

3.1. Pharmacokinetics of SPIO-alginate in normal rats

After injection of SPIO-alginate at both low dose and high dose, the blood iron concentration first gradually decreased from the maximal concentration at 0.083 h to the lowest concentration at 48 h (from 515.5 to 266.3 $\mu\text{g/mL}$ for SPIO-low dose group, and from 647.7 to 333.6 $\mu\text{g/mL}$ for SPIO-high dose group, respectively), and then recovered to the initial concentration before injection (about 471.9 $\mu\text{g/mL}$) at 96 h. In addition, the blood iron concentration after injection of alginate solution and saline also showed the similar profile (mildly down and up), and

Table 1
Serum iron concentration in rats after intravenous injection of SPIO-low dose (109.5 $\mu\text{mol Fe/kg}$), SPIO-high dose (218.9 $\mu\text{mol Fe/kg}$), 1 mL 0.6% (w/v) alginate solution, and saline. The basic serum iron concentration before administration was $10.64 \pm 4.58 \mu\text{g/mL}$. Data represent mean \pm S.D.

Time (h)	SPIO-low dose	SPIO-high dose	Alginate solution	Saline
0	9.32 ± 5.55	9.08 ± 3.42	10.96 ± 4.73	21.09 ± 6.13
0.083	143.75 ± 18.61	356.10 ± 42.82	6.16 ± 1.52	15.75 ± 3.71
0.167	131.90 ± 13.56	310.44 ± 64.55	5.48 ± 0.57	15.01 ± 1.18
0.5	57.62 ± 19.43	183.87 ± 37.37	7.49 ± 0.88	17.23 ± 2.23
1	19.57 ± 10.82	108.28 ± 38.23	8.52 ± 3.07	10.80 ± 1.88
3	8.74 ± 5.29	19.83 ± 15.31	6.86 ± 2.08	12.51 ± 5.25
6	6.79 ± 3.20	8.68 ± 5.36	4.72 ± 1.61	9.71 ± 0.92
12	3.28 ± 1.01	3.89 ± 2.13	6.96 ± 3.54	6.48 ± 1.23
24	4.52 ± 1.43	3.01 ± 1.75	5.07 ± 1.29	ND

ND: not determined.

the blood iron concentrations in all rats were even under the initial concentration before injection between 6 and 48 h after injection.

The basic serum iron concentration before administration fluctuated between 6.06 and 15.22 $\mu\text{g/mL}$. The serum iron concentrations at various time points after injection of alginate solution and saline located in the range of basic serum iron concentration (Table 1). But, the serum iron concentrations increased significantly after SPIO-alginate injection and then decreased to the basic serum iron concentration range at 3 h for low dose and at 6 h for high dose. The $T_{1/2}$ of SPIO-alginate was 0.27 ± 0.06 h at low dose and 0.65 ± 0.22 h at high dose calculated by noncompartmental analysis (Table 2).

3.2. Tissue distribution of SPIO-alginate in normal rats

Table 3 showed that the iron concentrations in liver and spleen significantly increased, while those in blood, lungs, heart, and kidneys slightly changed after injection of SPIO-alginate at low dose. Considering the weights of organs, the results revealed that more than 80% of the injected iron accumulated into the liver, and about 10% into the spleen while less than 2% was found in the kidneys, heart and lungs, respectively. The iron concentrations in the liver and the spleen were high between 0.5 and 24 h, and began to decrease after 24 h. The tissue distribution parameters in liver and spleen for SPIO-alginate in rat calculated

by the WinNonlin program using noncompartmental model was given in Table 2. It indicated that the elimination of iron in liver was slower than that in spleen.

3.3. Histological evaluation in normal rat

Although the experiments were carried out at different time points before and after injection of SPIO-alginate as described in methods, only the typical micrographs were shown in order to shorten the length of writing. HE staining could reflect the effect of SPIO-alginate on the morphology of tissues. The sections indicated that there was no significant change on the basic structure of all the specimens of liver and spleen, though there was a little edema of hepatocytes in the perimeter section of liver lobules (Fig. 1).

Perls staining was performed to detect the iron particles dyed blue. Stainable iron was observed in KCs in hepatic sinusoid, in splenic cord of the perimeter section of follicle and in splenic red pulp at 0.5, 24, 96, and 336 h after injection of low dose of SPIO-alginate (Fig. 1). Additionally, iron particles were distributed in the perimeter section of liver lobules at 0.5 h and in the center section at 96 h. The amount of iron oxide particles in liver qualitatively peaked between 0.5 and 24 h after injection, and small amounts of particles were still present at 336 h after injection. The results in the spleen were similar to those in the liver.

Table 2
Serum, liver and spleen parameters of SPIO-alginate in rats following intravenous injection at 109.5 and 218.9 $\mu\text{mol Fe/kg}$ using noncompartmental analysis with bolus IV administration for serum and extravascular administration for liver and spleen

Parameters	Serum ($n=5$)		Liver	Spleen
	Low dose	High dose	Low dose	Low dose
T_{max} (h)	0.083	0.083, 0.176	0.5	24
C_{max} ($\mu\text{g/mL}$ or g)	147.91 ± 20.72	$348.99 \pm 43.78^*$	176.64	290.06
λ (h^{-1}) ^a	2.95 ± 0.87	$1.28 \pm 0.40^*$	0.005	0.0085
$\text{AUC}_{0 \rightarrow 24\text{h}}$ ($\text{h } \mu\text{g/mL}$ or $\text{h } \mu\text{g/g}$) ^b	68.37 ± 18.87	$321.74 \pm 123.72^*$	35,176.83	26,307.97
$T_{1/2}$ (h)	0.25 ± 0.06	$0.59 \pm 0.20^*$	139.19	81.98
$\text{MRT}_{0 \rightarrow 24\text{h}}$ (h)	0.32 ± 0.11	$0.76 \pm 0.27^*$	181.179	86.235

Each value of serum parameter represents the mean \pm S.D.

^a $T_{1/2}$ was calculated from the terminal slope by means of log-linear regression.

^b AUC was calculated by linear trapezoidal rule.

* $P < 0.05$, compared with the value of low dose in serum.

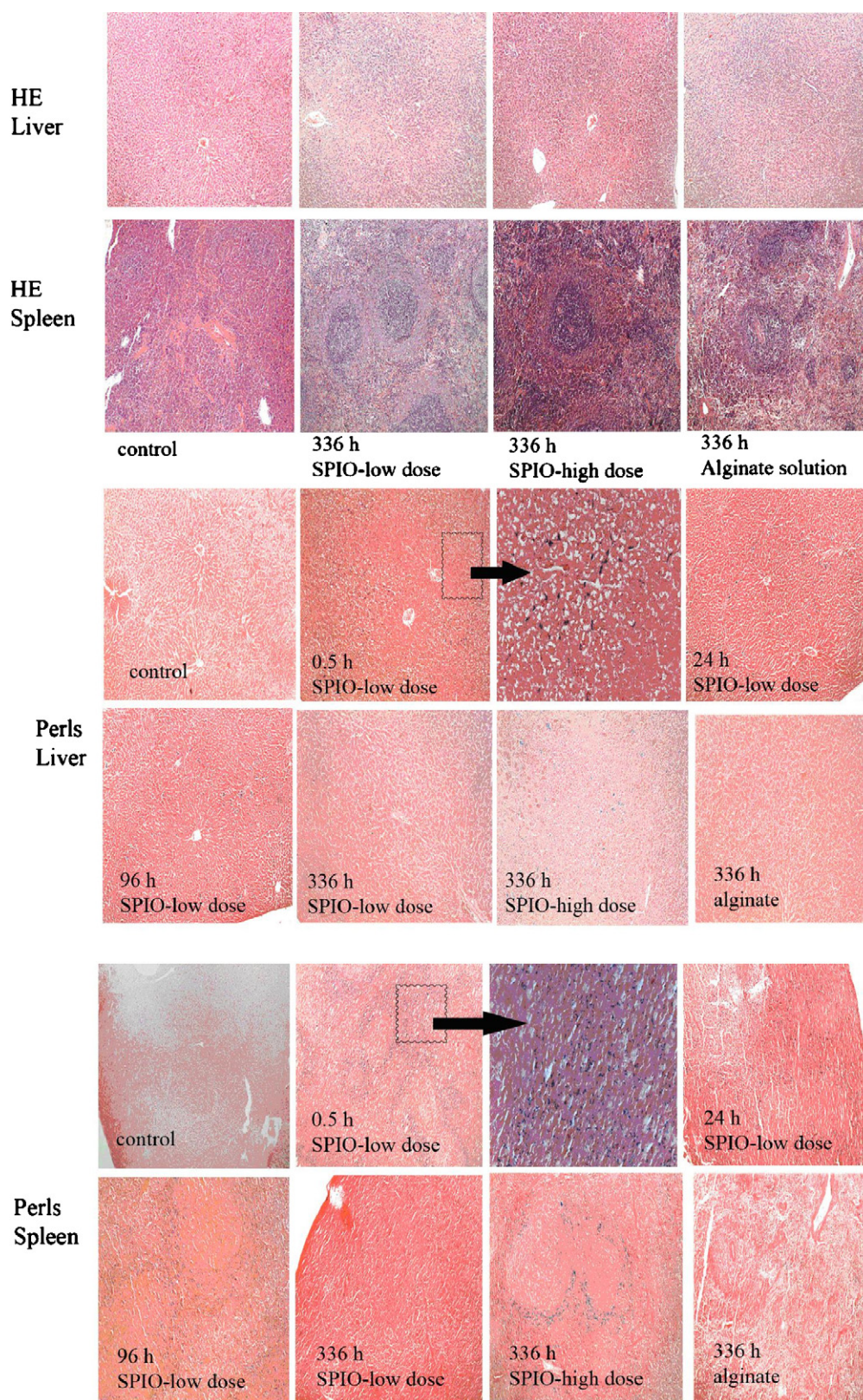


Fig. 1. Sections of liver and spleen of normal rat with HE staining and Perls staining (magnification $\times 10$).

Table 3
Iron concentration in different tissues at different timepoints after intravenous injection of SPIO-low dose (109.5 $\mu\text{mol Fe/kg}$). Data represent mean \pm S.D. ($n = 3$)

Time (h)	Iron concentrations in tissue ($\mu\text{g Fe/mL}$ in whole blood; $\mu\text{g Fe/kg}$ in heart, liver, spleen, lung, and kidney)					
	Whole blood	Liver	Spleen	Lung	Kidney	Heart
0	471.93 \pm 55.06	58.42 \pm 7.56	112.22 \pm 24.69	56.67 \pm 9.54	52.01 \pm 8.61	59.61 \pm 13.38
0.5	439.31 \pm 54.98	235.05 \pm 19.62	350.46 \pm 51.17	60.20 \pm 14.84	47.23 \pm 9.95	59.56 \pm 7.07
3	342.28 \pm 68.38	199.22 \pm 19.69	353.72 \pm 144.36	55.40 \pm 11.95	41.93 \pm 3.73	66.03 \pm 19.40
24	313.44 \pm 113.85	226.57 \pm 38.78	402.28 \pm 187.31	79.25 \pm 10.67	48.64 \pm 9.36	51.28 \pm 4.48
48	266.34 \pm 27.49	191.45 \pm 33.44	247.70 \pm 18.61	71.47 \pm 13.58	45.96 \pm 4.06	58.56 \pm 5.04
96	402.88 \pm 96.96	159.99 \pm 9.16	176.21 \pm 27.11	63.05 \pm 1.98	44.29 \pm 4.87	51.87 \pm 5.37
336	552.05 \pm 36.63	89.76	122.68	45.45	55.24	40.08

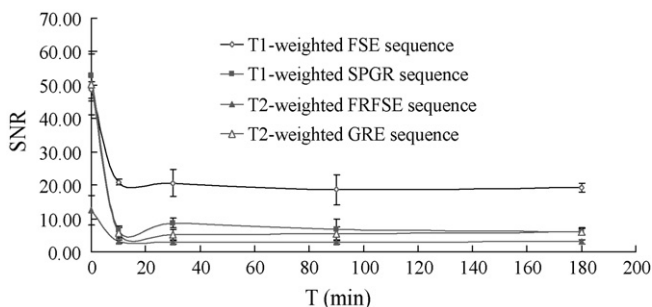


Fig. 2. *In vivo* SNR of liver in normal rats after injection of SPIO-alginate at a dose of 20 $\mu\text{mol Fe/kg}$. A negative enhancement was observed with T1-weighted, T2-weighted, and T2*-weighted sequences.

3.4. Liver enhancement of SPIO-alginate in normal rat

Fig. 2 showed the liver SNR before and after SPIO-alginate injection on both T1-weighted and T2-weighted images. Compared with unenhanced images ($t=0$), the SNR decreased at 10 min on T1-weighted FSE images, T1-weighted SPGR images, T2-weighted FRFSE images, and T2*-weighted GRE images, after SPIO-alginate injection, and remained almost stable up to 180 min, respectively. Hence, a remarkable negative enhancement was immediately obtained after the injection of SPIO-alginate.

3.5. MR imaging for rabbit tumor model

Fig. 3 showed the MR signal intensity of liver parenchyma (thick arrow) decreased, however, that of the tumor (fine arrow) did not obviously change and the borderline of the tumor was found more clearly in comparison with that of unenhanced

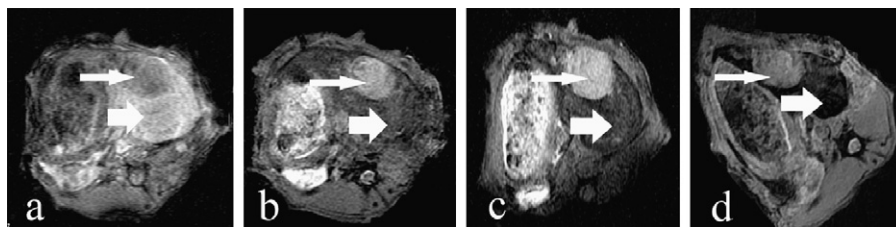


Fig. 3. T2*-weighted FSPGR images (TR/TE, 220 ms/5.2 ms) of xenograft liver cancer in rabbit at (a) 0 min (unenhanced imaging), (b) 10 min, (c) 30 min, and (d) 60 min after intravenous injection of SPIO-alginate at a dose of 20 $\mu\text{mol Fe/kg}$. After injection of SPIO-alginate, the liver parenchyma (thick arrow) showed a distinct signal loss, whereas that of the tumor (fine arrow) remained almost unaffected. Hence, the contrast between tumor and liver parenchyma was significantly increased.

image. The photograph and sections of rabbit VX2 tumor with Perls staining after MR imaging enhanced with SPIO-alginate were shown in Fig. 4. It was evident that there was a single tumor in the liver with the size of about 2.5 cm in accordance with that in MR images in Fig. 3. Iron oxide particles were observed in the normal part of liver rather than in the tumor (Fig. 4).

3.6. MR imaging for rats with primary liver cancer

During the process of establishing primary liver cancer model of rats, eight rats were dead because of hemorrhage in the tumor and poor resistance. In addition, two rats were chosen randomly and identified as cirrhosis at 12 weeks, and four rats were identified as HCC with cirrhosis at 15 weeks from MR imaging and pathological evaluation. Fifteen rats survived at 18 weeks in MR imaging experiment. All the fifteen rats were accompanied with severe cirrhosis, and no HCC was found in any rat on MR images before the injection of SPIO-alginate (pre-SPIO, unenhanced imaging). However, 22 HCCs were found in 11 rats after injection of SPIO-alginate (post-SPIO, enhanced imaging) and four rats were diagnosed as simple cirrhosis even after injection of SPIO-alginate. The $\text{SNR}_{\text{liver}}$ decreased from 48.95 ± 4.87 at pre-SPIO to 6.43 ± 3.37 at post-SPIO and the $\text{SNR}_{\text{cirrhosis}}$ from 45.51 ± 11.71 to 23.47 ± 7.52 . However, the SNR_{HCC} remained almost stable (45.51 ± 11.71 at pre-SPIO and 40.53 ± 12.98 at post-SPIO). Furthermore, the CNR of HCC increased from zero at pre-SPIO to 17.69 ± 3.69 at post-SPIO and the relative contrast increased from 1.0 at pre-SPIO to 1.79 ± 0.31 at post-SPIO. Hence, the contrast between HCC and liver parenchyma was significantly increased and the detection of HCC was improved.

In Fig. 5, compared with the signal intensity on unenhanced T2*-weighted GRE images, the liver signal intensity of nor-

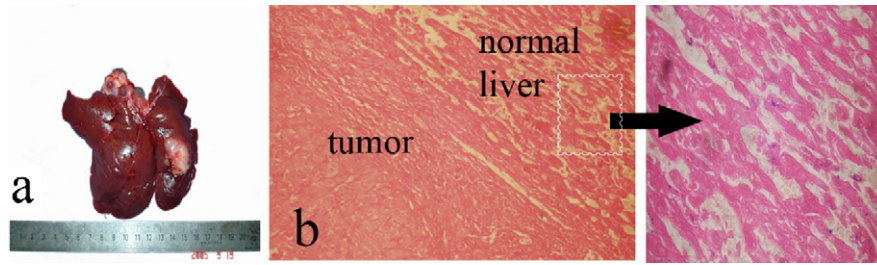


Fig. 4. Photographs (a) and sections of rabbit VX2 tumor with Perls staining (b) after MR imaging enhanced with SPIO-alginate. Iron oxide particles were not found in the tumor part, but in the normal part of the liver (magnification $\times 10$).

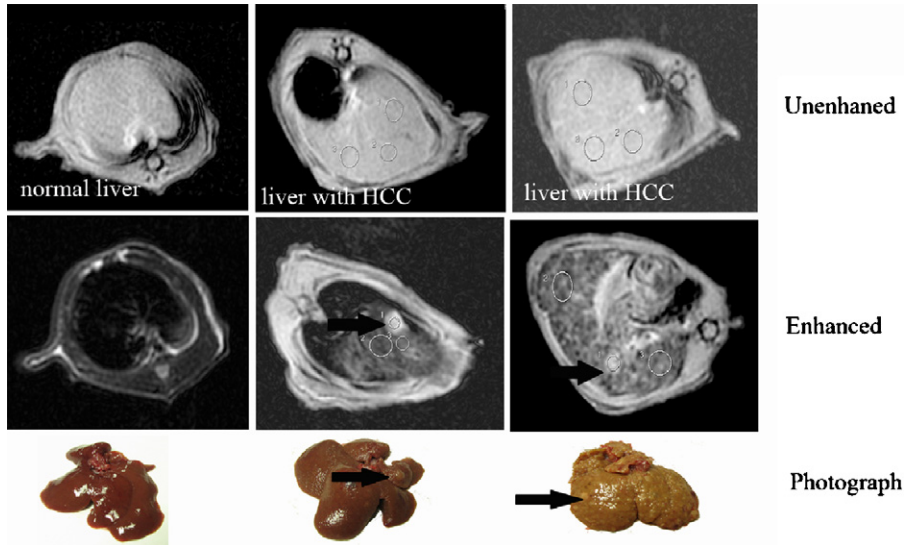


Fig. 5. T2*-weighted GRE images and photographs of liver with primary cancer in rats. No HCC was found on unenhanced images, however, some HCC were found (arrow) on SPIO-alginate enhanced images. The center photograph showed the liver of model rat has one HCC and slight cirrhosis, and the right-hand side photograph showed the liver of model rat has more HCC and severe cirrhosis.

mal rat on enhanced images decreased significantly, slightly decreased for cirrhosis, and almost did not decrease for HCC. Furthermore, there were hyperplastic nodules and some hemorrhage in photographs of model rats' liver. Fig. 6 showed the

sections of liver with Perls staining after MR imaging scan, ranging from 2 to 12 h after injection of 20 $\mu\text{mol Fe/kg}$ of SPIO-alginate, which indicated that iron oxide particles were present in normal liver, hyperplastic nodule and hemangioma, rather

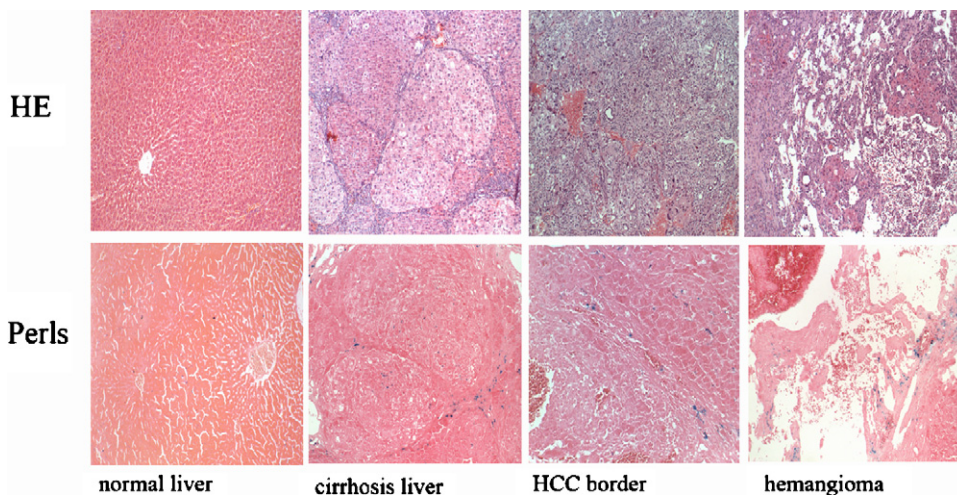


Fig. 6. Light micrograph with HE staining and Perls staining of liver in rats with primary cancer after MR imaging scan within 2–12 h after injection of 20 $\mu\text{mol Fe/kg}$ of SPIO-alginate. According to HE staining, the liver structure of control group was normal, and that of tumor model group accompanied with cirrhosis. Besides HCC, hyperplastic nodule, and hemangioma were identified. As for Perls staining, iron oxide particles were detected in the hemangioma and hyperplastic nodule, rather than in HCC (magnification $\times 10$).

than in HCC. All the livers of model rats were accompanied by cirrhosis according to HE staining. Meanwhile, some HCCs, hyperplastic nodules, and hemangiomas were identified.

4. Discussion

The alginate used in the study is of pharmaceutical grade which has been approved for oral administration as an inactive ingredient in human. Moreover, sodium alginate was studied for intravenous injection in some animals, and the LD₅₀ was described as less than 200 mg/kg for mouse, approximately 100 mg/kg for rabbit (Solandt, 1941), and 1000 mg/kg for rat (Sokov, 1970). In this study, the amounts of sodium alginate used in rats were about 40 mg/kg, which is far less than the LD₅₀ (Sokov, 1970). Furthermore, alginate is considered biocompatible and biodegradable in tissues. Alginate has been reported to undergo proton catalyzed hydrolysis which is dependent on time, pH, and temperature (Gombotz and Wee, 1998; Bouhadir et al., 2001; Robitaille et al., 1999). In addition, the chemical composition and the mitogenic contaminants found in alginate are the two main contributors to alginate immunogenicity including cytokine release and inflammatory reactions (Gombotz and Wee, 1998). Hence, the degradation of alginate in SPIO-alginate might result in the edema of hepatocytes.

Pharmacokinetics and tissue distribution of SPIO-alginate after intravenous injection were quantitatively studied by determining the iron concentration in blood, serum and tissues. Although it was difficult to differentiate between the endogenous iron and the injected iron, it was reliable to reflect the *in vivo* behavior of SPIO-alginate by subtracting the endogenous iron concentration and this method was used in some studies (Taupitz et al., 2004; Bourrinet et al., 2006). The phenomenon that the blood iron concentration values were under the initial concentration before injection (about 471.9 µg/mL) was observed from about 6 to 48 h after administration of SPIO-alginate, alginate solution and saline, was speculated these might be caused by the several bleedings. After several bleedings, red blood cell count would decrease and therefore there would be a decrease in iron content in blood samples. The blood iron concentration began to increase to initial level at 96 h after injection for both SPIO-alginate, which might be resulted from the fact that SPIO-alginate after uptake by macrophages was degraded by the lysosomes, and then the iron entered the plasma iron pool and was subsequently incorporated into red cell production (Pouliquen et al., 1991; Weissleder et al., 1989).

Since blood loss could significantly decrease red blood count and blood iron concentration, it was better to evaluate the pharmacokinetics of SPIO-alginate in serum, even though the basic serum iron concentration fluctuated according to different rats. In our study, the serum iron concentrations at various time points after injection of alginate solution were in the range of basic serum iron concentration (Table 1). Hence, it indicated that the intravenous injection of alginate solution had no effect on serum iron concentration. We speculated that the COO⁻ terminals of alginate might not bind the iron in serum. On the other hand, the half-life of SPIO-alginate in serum were 0.27 ± 0.05 h at 109.5 µmol Fe/kg and 0.65 ± 0.22 h at 218.9 µmol Fe/kg in rats

in Table 2. C_{\max} , $T_{1/2}$, AUC and MRT in serum with the high dose were significantly higher than those of the low dose ($P < 0.05$). After intravenous injection, SPIO-alginate accumulated dominantly in the liver and spleen with a total percentage of more than 90% (Table 3).

As an MR contrast agent, the physicochemical properties including the size of the particle, the charge and the nature of the coating, and the dose will determine the stability, distribution and metabolism of SPIO agents, and then will certainly affect MR imaging (Gupta and Gupta, 2005; Wang et al., 2001; Neuberger et al., 2005). According to the previous studies, the particle size played a very important role. The larger the particles, the shorter the plasma half-life is (Wang et al., 2001). Since SPIO uptake into the RES is related to protein absorption on the particle surface and subsequent opsonization, minimizing the particle size will ultimately reduce particle phagocytosis, finally resulting in a significant increase in plasma half-life and wider biodistribution (Neuberger et al., 2005). Although SPIO-alginate used in this research had a mean core diameter of about 5–10 nm, the big hydrodynamic diameter of 193.8 nm and high negative ξ -potential might explain the fast clearance from blood and the accumulation mostly in the liver and spleen (Table 2). This result was in accordance with the report that the blood half-life of Ferumoxides was 6 min and efficiently accumulated in the liver (approximately 80% of the injected dose) and spleen (5–10% of the injected dose) with minutes of administration (Wang et al., 2001). The amount of iron oxide (about 10–20 µmol Fe/kg body weight) for clinical MR imaging is small compared with other MR contrast agents and extensive toxicity studies in animals have indicated no acute or chronic toxicity at doses greater than 100 times the clinical effective dose (Weissleder et al., 1989; Reimer et al., 1995).

For specific characterization of liver lesions, the tissue-specific contrast agent should be located predominantly in one tissue. The distribution of contrast agent in liver is rather complicated, as it can be located in the extracellular space including blood and interstitium, and cellular space including reticuloendothelial cells, hepatocytes and endothelial cells. In our study, Perls staining did not show iron within hepatocytes but mainly within the KCs. Furthermore, the amount of SPIO-alginate in the liver peaked at 0.5 h with the dose of 109.5 µmol Fe/kg from quantitative iron concentration (Table 3) and qualitative histology evaluation (Fig. 1). This suggested that SPIO-alginate could not act as an extracellular agent during the early time points. These results were in accordance with the liver enhancement of SPIO-alginate in normal rat, in which a significant decrease of the liver signal intensity on T1-weighted images at 10 min was observed (Fig. 2). It was reported that positive enhancement on T1-weighted images was observed when the iron particles were extracellular. When the particles were intracellular, only a negative enhancement was seen (Oswald et al., 1997; Van Beers et al., 2001). It was suggested that the uptake of contrast agents of negative ξ -potential was mediated by scavenger receptors expressed in both Kupffer and liver endothelial cells (Seternes et al., 2001). Compared to KCs, liver endothelial cells were believed to be less effective at metabolizing and degrading particulate iron (Briley-Sæbø et al., 2004). The half life of SPIO-alginate in

liver at a dose of 109.5 $\mu\text{mol Fe/kg}$ was about 139.1 h (Table 2) and only small iron was observed at 336 h after injection from Perls staining (Fig. 1). Hence, we speculated that there was little or almost no SPIO-alginate in endothelial cell. In sum, the distribution of SPIO-alginate in liver was predominately in KCs, which was just the mechanism of SPIO-alginate to detect liver tumors.

A negative enhancement of the liver was observed on both T1- and T2-weighted images after injection of SPIO-alginate in normal rats (Fig. 2). Compared with the corresponding unenhanced images, SNR on enhanced images decreased by 2.32 times with T1-weighted FSE sequence, 8.02 times with T1-weighted SPGR sequences, 3.88 times with T2-weighted IRFSE sequence, and 8.64 times with T2*-weighted GRE sequence. The negative enhancement on T1-weighted images might be caused by the physical characteristics of the individual nanoparticles. In other words, the high-field magnetization of the iron oxide core could be sufficient to relax water protons effectively, which might attribute to the fact that iron oxide was not simply coated by alginate polymer (Ma et al., 2007). Furthermore, the results also indicated that SPIO-alginate did not agglomerate *in vivo* (Kellar et al., 2002). Meanwhile, the intracellular iron particles mentioned above might be another reason for the negative enhancement on T1-weighted images. On the other hand, the negative enhancement effect of SPIO-alginate on T2- and T2*-weighted images was demonstrated, and GRE images were more sensitive to susceptibility effects than FSE images according to earlier report (Ward et al., 2003).

SPIO-alginate was mainly phagocytosed by liver after intravenous administration as mentioned above. As a result, these particles taken up in liver could accelerate T2 relaxation by creating local inhomogeneities in the magnetic field, causing reduced signal intensity on both T1- and T2-weighted images, but most remarkable decrease on acquisitions with T2*-weighted. In this study, HCC was not found at pre-SPIO on T2*-weighted images, but found at post-SPIO, for the signal intensity of HCC was significantly higher than that of the adjacent liver parenchyma (Fig. 5). Hence, MR imaging with SPIO-alginate enhancement was shown to improve the detection of HCC in the cirrhotic liver compared with unenhanced imaging. Our study confirmed these expectations, as did most published studies of the recent years (Saini et al., 1987; Clement et al., 1991; Nakayama et al., 1998; Imai et al., 2000; Bourrinet et al., 2006).

The efficacy of iron oxide to enhance the transverse relaxation rates ($1/T2^* = R2^*$) in the liver depended upon its initial distribution or uptake into the liver. Factors which may alter the uptake of SPIO particles and the resultant effect on signal intensity include phagocytic activity, clustering of the particles, and local blood flow.

First of all, the change of signal intensity in liver on SPIO enhanced MR imaging is mainly mediated by phagocytic activity. And phagocytic activity is depended on both the number of sinusoidal KCs per unit volume of liver parenchyma (KCs tissue density) and individual KCs function. It is suggested that the number of KCs in dysplastic nodules or in cirrhosis is similar to that in adjacent liver parenchyma, and the number of KCs in HCC decreased as the tumors became less well

differentiated (Imai et al., 2000). It has been reported that SPIO-enhanced MR imaging can evaluate the number and function of KCs (Tanimoto et al., 2002). In our studies, iron oxide particles were found in normal liver and hyperplastic nodule, rather than in HCC and VX2 tumor from histological evaluation (Figs. 4 and 6).

It has been reported that the signal intensity changes induced by SPIO may vary according to the spatial distribution of particles and cluster size on relaxation times within KCs in T2*-weighted sequences and T2*-insensitive weighted sequences (Imai et al., 2000). Additionally, large intracellular SPIO clusters produced greater SNR loss on GRE images than small clusters because of the magnetic susceptibility effects relating to fixed-field inhomogeneity. In contrast, small intracellular clusters caused little SNR decrease on T2*-weighted GRE images while the small clusters produced substantial SNR loss on T2-weighted FSE images. This could attribute to T2 shortening mechanisms that were independent of magnetic susceptibility effects but relate to the greater free water interaction made possible by the relatively larger surface area of the small clusters (Tanimoto et al., 1994; Tanimoto et al., 2001). However, the size of the intracellular SPIO clusters depended on individual KC phagocytic function. Hence, impaired phagocytic activity, as in liver cirrhosis, should be associated with a decreased average size of SPIO clusters within KC. In this study, SNR of the normal liver of control rats with T2*-weighted GRE sequence decreased by about eight times on SPIO-enhanced images, while twice as that of the cirrhosis liver of model rats. This result was consistent with those reports that the signal intensity induced by SPIO in patients with liver cirrhosis was less remarkable than that in non-cirrhotic patients (Hundt et al., 2000; Clement et al., 1991; Nakayama et al., 1998). Hemangiomas could show SPIO uptake because of the blood pool effect, although they do not contain KCs (Kim et al., 2002). It was obvious that there were many iron oxide particles stainable in hemangiomas in Fig. 6. Therefore, hemangiomas could not be identified on T2*-weighted MR images.

5. Conclusion

The SPIO-alginate was cleared rapidly from serum with the half-life of 0.27 h at 109.5 $\mu\text{mol Fe/kg}$ and accumulated dominantly in the liver and spleen with a total percentage of more than 90% after intravenous injection. Iron oxide particles in KCs as well as splenic red pulp were observed from histological evaluation in normal rats. The experiments on MR imaging indicated that SPIO-alginate as an MR contrast agent might have the ability to improve detection of liver tumor.

Acknowledgements

This work was supported by funds from National High Technology Research and Development Program of China (2003AA326020), National Basic Research Program of China 2007CB935801, and National Natural Science Foundation of China (30772665).

References

- Bouhadir, K.H., Lee, K.Y., Alsberg, E., Damm, K.L., Anderson, K.W., Mooney, D.J., 2001. Degradation of partially oxidized alginate and its potential application for tissue engineering. *Biotechnol. Prog.* 17, 945–950.
- Bourrinet, P., Bengele, H.H., Bonnemain, B., Dencausse, A., Idee, J.M., Jacobs, P.M., Lewis, J.M., 2006. Preclinical safety and pharmacokinetic profile of Ferumoxtran-10, an ultrasmall superparamagnetic iron oxide magnetic resonance contrast agent. *Invest. Radiol.* 41, 313–324.
- Briley-Sæbø, K., Hustvedt, S.O., Haldorsen, A., Bjørnerud, A., 2004. Long-term imaging effects in rat liver after a single injection of an iron oxide nanoparticle based MR contrast agent. *J. Magn. Reson. Imaging* 20, 622–631.
- Clement, O., Frija, G., Chambon, C., Schouman-Clayes, E., Mosnier, J.F., Poupon, M.F., Balkau, B., 1991. Liver tumors in cirrhosis: experimental study with SPIO-enhanced MR imaging. *Radiology* 180, 31–36.
- Corot, C., Robert, P., Idee, J.M., Port, M., 2006. Recent advances in iron oxide nanocrystal technology for medical imaging. *Adv. Drug Deliv. Rev.* 58, 1471–1504.
- Gombotz, W.R., Wee, S.F., 1998. Protein release from alginate matrices. *Adv. Drug Deliv. Rev.* 31, 267–285.
- Gupta, A.K., Gupta, M., 2005. Synthesis and surface engineering of iron oxide nanoparticles for biomedical applications. *Biomaterials* 26, 3995–4021.
- Hagar, W., Vichinsky, E.P., Theil, E.C., 2003. Liver ferritin subunit ratios in neonatal hemochromatosis. *Pediatr. Hematol. Oncol.* 20, 229–235.
- Harmut-Hoene, A., Schelenz, R., 1980. Effect of dietary fiber on mineral absorption in growing rats. *J. Nutr.* 110, 1774–1784.
- Hauff, P., Fritsch, T., Reinhardt, M., Weitschies, W., Lueders, F., Uhlendorf, V., Heldmann, D., 1997. Delineation of experimental liver tumors in rabbits by a new ultrasound contrast agent and stimulated acoustic emission. *Invest. Radiol.* 32, 94–99.
- Hundt, W., Petsch, R., Helmberger, T., Reiser, M., 2000. Signal changes in liver and spleen after Endorem administration in patients with and without liver cirrhosis. *Eur. Radiol.* 10, 409–416.
- Imai, Y., Murakami, T., Yoshida, S., Nishikawa, M., Ohsawa, M., Tokunaga, K., Murata, M., Shibata, K., Zushi, S., Kurokawa, M., Yonezawa, T., Kawata, S., Takamura, M., Nagano, H., Sakon, M., Monden, M., Wakasa, K., Nakamura, H., 2000. Superparamagnetic iron oxide-enhanced magnetic resonance images of hepatocellular carcinoma: correlation with histological grading. *Hepatology* 32, 205–212.
- Kellar, K.E., Fujii, D.K., Gunther, W.H.H., Briley-Sæbo, K., Bjørnerud, A., Spiller, M., Koenig, S.H., 2002. Important considerations in the design of iron oxide nanoparticles as contrast agents for T1-weighted MRI and MRA. *Acad. Radiol.* 9, S34–S37.
- Kellar, K.E., Fujii, D.K., Gunther, W.H.H., Briley-Sæbo, K., Bjørnerud, A., Spiller, M., Koenig, S.H., 2000. “NC100150 injection,” a preparation of optimized iron oxide nanoparticles for positive contrast MR angiography. *J. Magn. Reson. Imaging* 11, 488–494.
- Kim, J.H., Kim, M.J., Suh, S.H., Chung, J.J., Yoo, H.S., Lee, J.T., 2002. Characterization of focal hepatic lesions with ferumoxides-enhanced MR imaging: utility of T1-weighted spoiled gradient recalled echo images using different echo times. *J. Magn. Reson. Imaging* 15, 573–583.
- Ma, H.L., Qi, X.R., Maitani, Y., Nagai, T., 2007. Preparation and characterization of superparamagnetic iron oxide nanoparticles stabilized by alginate. *Int. J. Pharma* 333, 177–186.
- Ma, H.L., Qi, X.R., Ding, W.X., Maitani, Y., Nagai, T., 2007a. Magnetic targeting after femoral artery administration and biocompatibility assessment of superparamagnetic iron oxide nanoparticles. *J. Biomed. Mater. Res. Part A* 84A, 598–606.
- Nakayama, M., Kamura, T., Kimura, M., Seki, H., Tsukada, K., Sakai, K., 1998. Quantitative MRI of hepatocellular carcinoma in cirrhotic and noncirrhotic livers. *Clin. Imaging* 22, 280–283.
- Neuberger, T., Schöpf, B., Hofmann, H., Hofmann, M., Von Rechenberg, B., 2005. Superparamagnetic nanoparticles for biomedical applications: Possibilities and limitations of a new drug delivery system. *J. Magn. Mater.* 293, 483–496.
- Oswald, P., Clement, O., Chambon, C., Schouman-Clayes, E., Frija, G., 1997. Liver positive enhancement after injection of superparamagnetic nanoparticles: respective role of circulating and uptaken particles. *Magn. Reson. Imaging* 15, 1025–1031.
- Pouliquen, D., Le Jeune, J.J., Perdriset, R., Ermias, A., Jallet, P., 1991. Iron oxide nanoparticles for use as an MRI contrast agent: pharmacokinetics and metabolism. *Magn. Reson. Imaging* 9, 275–283.
- Reimer, P., Rummeny, E.J., Daldrup, H.E., Balzer, T., Tombach, B., Berns, T., Peters, P.E., 1995. Clinical results with resovist: a phase 2 clinical trial. *Radiology* 195, 489–496.
- Robitaille, R., Pariseau, J.F., Leblond, F.A., Lamoureux, M., Lepage, Y., Hallé, J.P., 1999. Studies on small (<350 µm) alginate-poly-L-lysine microcapsules. III. Biocompatibility of smaller versus standard microcapsules. *J. Biomed. Mater. Res.* 44, 116–120.
- Saini, S., Stark, D.D., Hahn, P.F., Bousquet, J.C., Introcasso, J., Wittenberg, J., Brady, T.J., Ferrucci J.T.Jr., 1987. Ferrite particles: a superparamagnetic MR contrast agent for enhanced detection of liver carcinoma. *Radiology* 162, 217–222.
- Seternes, T., Oynebraten, I., Sorensen, K., Smedsrod, B., 2001. Specific endocytosis and catabolism in the scavenger endothelial cells of cod (*Gadus morhua* L.) generate high-energy metabolites. *J. Exp. Biol.* 204, 1537–1546.
- Sokov, L.A., 1970. Radioaktivnye Izotopy Vo Vneshnei Sredei Organizine. Atomizdat, Moscow, p. 247.
- Soland, O.M., 1941. Some observations upon sodium alginate. *Quart. J. Exp. Physiol.* 31, 25–30.
- Tanimoto, A., Pouliquen, D., Kreft, B.P., Stark, D.D., 1994. Effects of spatial distribution on proton relaxation enhancement by particulate iron oxide. *J. Magn. Reson. Imaging* 4, 653–657.
- Tanimoto, A., Oshio, K., Suematsu, M., Pouliquen, D., Stark, D.D., 2001. Relaxation effects of clustered particles. *J. Magn. Reson. Imaging* 14, 72–77.
- Tanimoto, A., Yuasa, Y., Shinmoto, H., Jinzaki, M., Imai, Y., Okuda, S., Kuribayashi, S., 2002. Superparamagnetic iron oxide-mediated hepatic signal intensity change in patients with and without cirrhosis: pulse sequence effects and Kupffer cell function. *Radiology* 222, 661–666.
- Taupitz, M., Wagner, S., Schnorr, J., Kravec, I., Pilgrimm, H., Bergmann-Fritsch, H., Hamm, B., 2004. Phase I clinical evaluation of citrate-coated monocrySTALLINE very small superparamagnetic iron oxide particles as a new contrast medium for magnetic resonance imaging. *Invest. Radiol.* 39, 394–405.
- Van Beers, B.E., Sempoux, C., Materne, R., Delos, M., Smith, A.M., 2001. Biodistribution of ultrasmall iron oxide particles in the rat liver. *J. Magn. Reson. Imaging* 13, 594–599.
- Wang, Y.X., Hussain, S.M., Krestin, G.P., 2001. Superparamagnetic iron oxide contrast agents: physicochemical characteristics and applications in MR imaging. *Eur. Radiol.* 11, 2319–2331.
- Ward, J., Guthrie, J.A., Wilson, D., Arnold, P., Lodge, P., Toogood, G.J., Wyatt, J.I., Robinson, P.J., 2003. Colorectal hepatic metastases: detection with SPIO-enhanced breath-hold MR imaging-comparison of optimized sequences. *Radiology* 228, 709–718.
- Weinmann, H.J., Ebert, W., Misselwitz, B., Schmitt-Willich, H., 2003. Tissue-specific MR contrast agents. *Eur. J. Radiol.* 46, 33–44.
- Weissleder, R., Stark, D.D., Engelstad, B.L., Bacon, B.R., Compton, C.C., White, D.L., Jacobs, P., Lewis, J., 1989. Superparamagnetic iron oxide: pharmacokinetics and toxicity. *Am. J. Roentgenol.* 152, 167–173.